Chinese Chemical Letters 37 (2026) 111429

Contents lists available at ScienceDirect

Chinese Chemical Letters

journal homepage: www.elsevier.com/locate/cclet

Carbon–metal bond homolysis-recombination enabling enantioconvergent carboxylation with CO_2: A theoretical study

Qi Zhou[a], Cefei Zhang[a], Hui-Lin Luo[a], Chuan-Xi Nie[a], Changwei Hu[a], Jian-Heng Ye[a], Zhishan Su[a,*], Li-Li Liao[b,*], Da-Gang Yu[a,c,*]

[a] Key Laboratory of Green Chemistry & Technology of Ministry of Education, College of Chemistry, Sichuan University, Chengdu 610064, China
[b] West China School of Public Health and West China Fourth Hospital, Sichuan University, Chengdu 610041, China
[c] State Key Laboratory of Coordination Chemistry, School of Chemistry and Chemical Engineering, Nanjing University, Nanjing 210023, China

ARTICLE INFO

Article history:
Received 23 April 2025
Revised 22 May 2025
Accepted 8 June 2025
Available online 9 June 2025

Keywords:
Enantioconvergent carboxylation
Carbon–metal bond homolysis-recombination
Transition metal catalysis
DFT calculation
Theoretical study

ABSTRACT

The generation of transient radical species *via* carbon–metal bond homolysis is extremely useful, which can be harnessed to promote useful and selective radical-type transformations by the combination of transition metal catalysis. We herein establish a carbon–metal bond homolysis/recombination model for the formation of enantiomerically enriched carbon-metal species, which accounts for the Ni-catalyzed enantioconvergent carboxylation of racemic benzyl ammonium salts with CO_2. Theoretical studies suggest a distinct pathway involving a stereoinvertive nucleophilic substitution-type oxidative addition of racemic benzyl ammonium salts to Ni(0), forming a racemic benzyl Ni(II) intermediate. Subsequent C–Ni bond homolysis of one enantiomer enables the formation of a transient radical, followed by a dynamic rotation along C–C$^{\bullet}$ bond and radical recombination forming another more thermodynamically favored enantiomer. Geometry analysis suggests less H–H repulsion between the benzyl group and chiral ligand in the more stable isomer. After the reduction and stereoretentive inner-sphere nucleophilic attack on CO_2 process, the desired enantiomerically enriched carboxylic acid product is generated. ETS-NOCV analysis reveals a significant back-donation interaction between the $d_{x2\text{-}y2}$ orbital of Ni atom and the unoccupied π^* orbital of CO_2 in inner-sphere transition state, thus effectively stabilizing the Ni–CO_2 complex and facilitating subsequent C–C bond formation. The theoretical calculations provide critical insights into the systematic development of transition metal-catalyzed asymmetric carboxylation, highlighting significant potential for broad applications in synthetic organic chemistry.

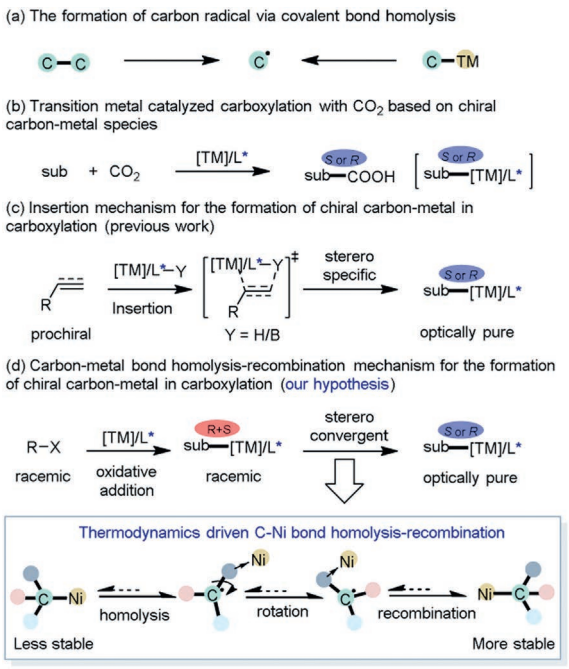
© 2026 Published by Elsevier B.V. on behalf of Chinese Chemical Society and Institute of Materia Medica, Chinese Academy of Medical Sciences.

Radicals are exceptionally reactive intermediates that readily engage with a wide array of organic molecules [1–4]. Their defining characteristic lies in their rapid reactivity, often occurring at diffusion-limited rates. While this property enables efficient substrate activation, it also presents challenges in achieving selective control, particularly in the context of enantioselective transformations. Among these, the carbon radical has been established as a crucial intermediate for C–C bond formation, attracting significant attention [5–7]. Covalent bond homolysis has been demonstrated as a versatile method for carbon radical generation (Scheme 1a) [8–16]. Homolytic cleavage of a C–C bond by high-temperature thermolysis or ultraviolet irradiation has been employed to generate radical pairs [8,9]. Similarly, homolytic cleavage of a carbon-metal bond in alkyl metal compounds may take place, making it prone to generating transient radical species [10–15]. Especially when the metals exhibit spin diversity, such as Fe [11], Co [12], and Ni [13,14] in the early transition metals of the fourth period, the phenomenon becomes particularly noteworthy. The generation of transient radical species *via* carbon–metal bond homolysis is highly valuable, as it can be strategically leveraged to facilitate selective and efficient radical-type transformations in conjunction with transition metal catalysis [16,17].

Recently, transition metals, including Ni, Cu, Rh, and Pd, catalyzed asymmetric carboxylation with carbon dioxide (CO_2) have attracted much attention as a complementary method to construct important chiral carboxylic acids (Scheme 1b) [18–22]. These transformations usually involve the generation of an optically pure enantiomeric carbon-metal species as the key intermediate for CO_2 transformation and enantioselectivity control. From a theoretical perspective, π-bond insertion of a prochiral substrate into a metal-hydride/boron bond stereospecifically generates an optically pure enantiomeric carbon-metal species efficiently [23–26]. In

* Corresponding authors.
E-mail addresses: suzhishan@scu.edu.cn (Z. Su), liaolili94@scu.edu.cn (L.-L. Liao), dgyu@scu.edu.cn (D.-G. Yu).

https://doi.org/10.1016/j.cclet.2025.111429
1001-8417/© 2026 Published by Elsevier B.V. on behalf of Chinese Chemical Society and Institute of Materia Medica, Chinese Academy of Medical Sciences.



Scheme 1. The formation of chiral carbon-metal species in transition metal-catalyzed carboxylation with CO_2. TM = transition metal, L = ligand, sub = substrate.

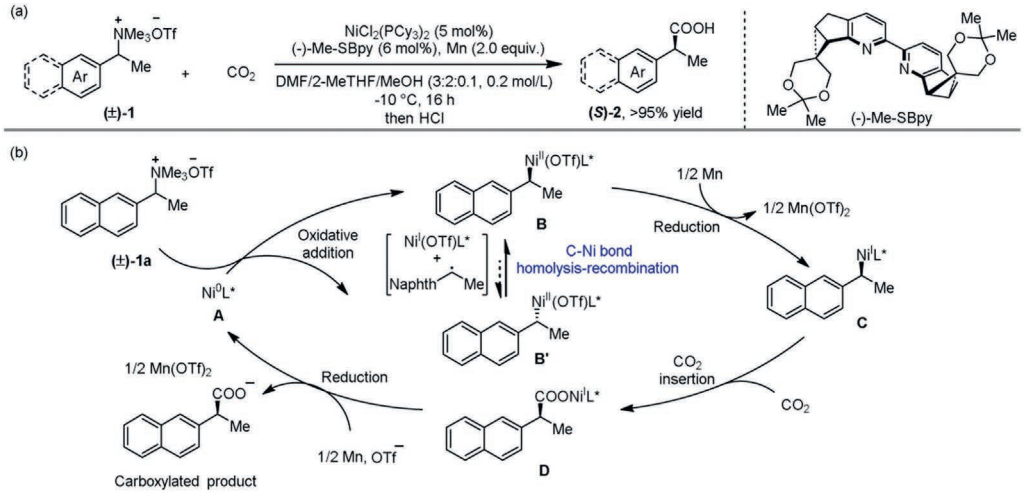
this case, substrates such as alkenes and alkynes can participate in transition-metal catalyzed asymmetric carboxylation with CO_2 pioneered by Mori [27], Mikami [28], Yu [26,29–34], Tang, and Zhou [35,36] groups, by constructing alkyl- or alkenyl–metal species that can be directly transformed into various central or axial chiral carboxylic acids (Scheme 1c).

In addition to the π-bond insertion strategy which is effective for both alkenes and alkynes in generating carbon-metal species, an alternative approach known as oxidative addition facilitates the formation of carbon-metal species from electrophiles such as alkyl (pseudo)halides [30,37–39]. Nevertheless, oxidative addition of a racemic alkyl (pseudo)halide to a low-valent transition metal usually results in the generation of a racemic carbon-metal species. One potential way to obtain optically pure enantiomeric carbon-metal species may involve the homolysis of the carbon-metal bond. The homolytic process is inherently thermodynamically endergonic, resulting in the formation of a transient radical. The transient nature and inherent reactivity of the radical facilitate the dynamic rotation along the C–C• bond achieving an isomerization process. After recombination with metal species, another stereoconfigurated carbon-metal species can be generated. This means upon generation of racemic carbon-metal species, one enantiomer may convert into another more thermodynamically stable one. We propose that applying this protocol to organo (pseudo)halides could provide chiral carboxylated products by the generation of optically pure enantiomeric carbon–metal species. Herein, we report the theoretical study on enantioconvergent carboxylation with CO_2 based on carbon-metal bond homolysis/recombination model (Scheme 1d).

To address the above issues, we conducted theoretical investigations and chose Ni-catalyzed enantioconvergent carboxylation of alkyl ammonium salts with CO_2 reported by Li's research group as the model reaction (Scheme 2a) [40]. Their experimental exploration showed that this carboxylation could be achieved in the presence of a Ni catalyst, the chiral ligand Me–SBpy, and manganese (Mn) powder under one atmosphere of CO_2. It was found that the excellent yields and enantioselectivities were almost obtained for two separate reactions whether using (*S*)- or (*R*)-alkyl ammonium salt **1a**, indicating a racemization step before generating a chiral alkyl Ni complex. This study aims to verify the carbon-metal bond homolysis/recombination model for Ni-catalyzed enantioconvergent carboxylation with CO_2, providing direction for the rational design of Ni-catalyzed enantioconvergent carboxylation reactions, which are attractive for synthetic applications.

On the basis of literature [40,41] and our proposed model, we proposed the mechanistic cycle for the Ni-catalyzed enantioconvergent carboxylation of alkyl ammonium salts with CO_2, as shown in Scheme 2b. In this process, Ni(0) complex is considered to the active catalytic species. Oxidative addition of the racemic ammonium salt **1a** to Ni(0) complex **A** generates benzylic Ni(II) intermediates **B** and **B'** as two enantiomers. Then, C–Ni bond homolysis-recombination occurs, facilitating the formation of a thermodynamically stable enantiomer. The resulting optically pure enantiomeric Ni(II) complex could be reduced by Mn(0) to generate Ni(I) species **C**. This is followed by the insertion of CO_2 into the C–Ni(I) bond, leading to the formation of Ni(I) carboxylate intermediate **D**. Further reduction then regenerates the Ni(0) species **A** and releases the carboxylated product.

All structures in this study were optimized using the Gaussian 09 package [42], employing the B3LYP-D3(BJ) [43,44] functional in the *N*,*N*-dimethylformamide (DMF) solvent. The relative effective core potential (ECP) in combination with the LanL2DZ



Scheme 2. (a) Model reaction. (b) Possible mechanism for the Ni-catalyzed enantioconvergent carboxylation of alkyl ammonium salts with CO_2. Naphth = Naphthyl group.

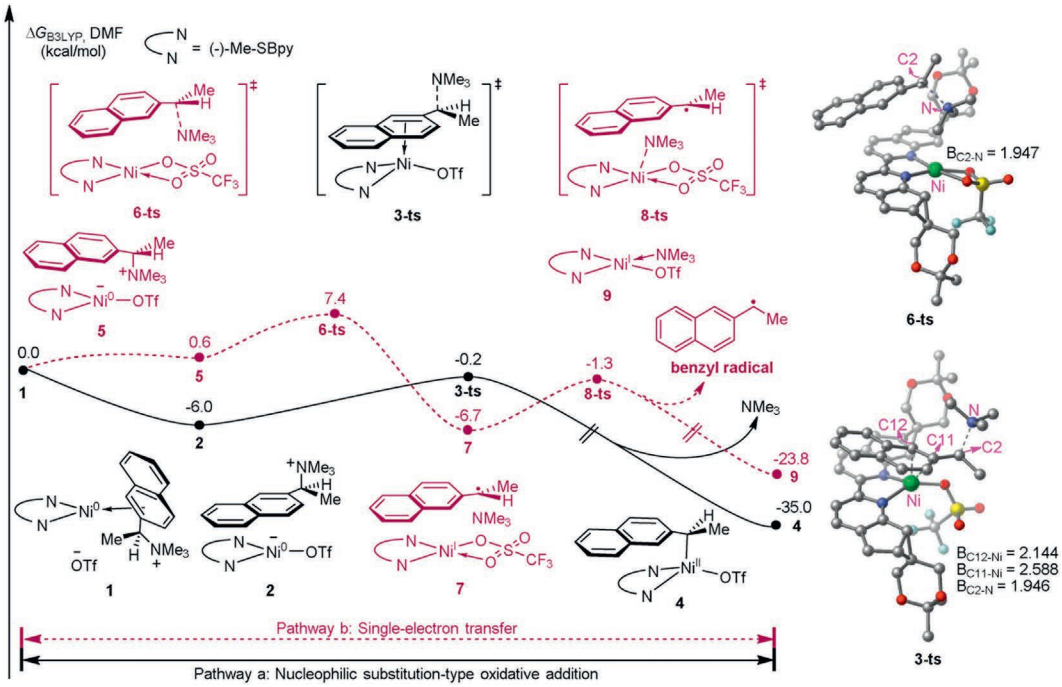


Fig. 1. Energy profiles for the C(benzyl)–N bond activation with a Ni(0) complex *via* nucleophilic substitution-type oxidative addition and single-electron transfer (all energies are in kcal/mol) and optimized geometries of **3-ts** and **6-ts** (all distances are given in angstrom).

[45–47] basis set was employed for Ni and Mn atoms, whereas the 6–31G(d) basis set [48] was assigned to all remaining atoms. Thermodynamic energy corrections were obtained at 298 K. Frequency analysis was conducted to confirm that the optimized geometries corresponded to a minimum (with no imaginary frequencies) or a transition state (with exactly one imaginary frequency). The solvent effect was evaluated using the self-consistent reaction field (SCRF) method and the SMD model [49]. Intrinsic reaction coordinate (IRC) [50] calculations were performed to verify the transition state (TS) associated with the corresponding minimum on the potential energy surface. Single-point energy calculations were carried out at the B3LYP-D3(BJ)/[SDD, 6–311+G(d,p)](SMD, DMF) level of theory [51,52]. Optimized molecular structures were visualized with CYLview (version 2.0) [53]. To gain further insight into the electron properties of key species in the reaction, natural bond orbital (NBO) analysis was carried out at the same level of theory as the structural optimization [54,55]. The extended transition state-natural orbitals for chemical valence (ETS-NOCV) [56–59] analysis was performed with Multiwfn 3.8 (dev) software [60], and the corresponding results were visualized using VMD software [61].

A detailed density functional theory (DFT) calculation was performed to investigate the mechanism of the Ni-catalyzed enantioconvergent carboxylation, which was initiated with oxidative addition. As shown in Fig. 1, the Ni(0) complex **1** generated by coordination with (*S*)-ammonium salt **1a** was considered as the zero point of the free energy profiles. Owing to the features of the Ni(0) complex and the alkyl (pseudo)halides [62–64], two possible pathways for the oxidative addition of C(benzyl)–N bond were proposed and investigated, including nucleophilic substitution-type C–N oxidative addition (pathway a) and single-electron transfer (pathway b) [65]. We failed to locate three membered-ring oxidative addition transition state, likely due to steric hindrance. First, we calculated the activation free energy for the nucleophilic substitution-type C(benzyl)–N bond oxidative addition with the Ni(0) complex to deliver benzyl-Ni(II) complex **4** (pathway a). This nucleophilic substitution step *via* transition state **3-ts**, featuring a triplet state at the Ni center, has an energy barrier of 5.8 kcal/mol. Geometry analysis shows that the length of C2–N, C11–Ni, C12–Ni bonds in **3-ts** are 1.946, 2.588, and 2.144 Å, respectively, indicating a coordination of Ni center to naphthalene group. Pathway b involves a radicophilic Ni(0) center [63], which undergoes single-electron transfer to form a benzyl radical through the breaking of the C(benzyl)–N bond. The relative free energy of **6-ts** is calculated as 7.4 kcal/mol. Geometry analysis shows that the length of C2–N bond in **6-ts** is 1.947 Å, and the spin population of Ni atom and the total benzyl group is −0.907 and 0.562, respectively. The relative free energy of transition state **3-ts** is 7.6 kcal/mol lower than that of transition state **6-ts**. Therefore, nucleophilic substitution-type oxidative addition *via* **3-ts** is the dominant pathway according to our computational results, being exoergic by 35.0 kcal/mol for the generation of (*R*)-benzylic Ni(II) intermediate **4** (Figs. S2 in Supporting information).

We then investigated how the enantiomeric carbon-metal species was formed. Our calculations using (*S*)-ammonium salt **1a** ligated with Ni(0) species demonstrate the generation of benzyl Ni(II) complex **4** *via* configuration reversal nucleophilic substitution-type oxidative addition transition state **3-ts**. In experimental observations, TEMPO-benzyl adduct and benzyl radical homocoupling side product were detected in the reaction system mechanistic studies, indicating the formation of a benzyl radical. We proposed that the homolysis of C2–Ni bond in **4** could form benzyl radical and Ni(I) species. This process *via* aryl-ring coordinated C–Ni bond homolysis transition state **10-ts** requires an energy barrier of 8.0 kcal/mol, leading to the formation of Ni(I) species **11**. Geometry analysis shows that the lengths of C2–Ni, C11–Ni and C12–Ni bonds in **11** are 3.091, 2.575 and 2.153 Å, respectively, indicating an η^2-coordination of Ni center (Fig. S4c in Supporting information). Moreover, spin population analysis of **11** shows spin densities of 0.522, −0.162, 0.252 and 1.217 on the C2, C11, C12 and Ni atoms, respectively, indicating the radical character of benzyl fragment. Furthermore, we located the transition states **12-ts** associated with the C–C bond rotation in intermediate **11**. The energy barrier *via* **12-ts** is 16.5 kcal/mol, indicating that

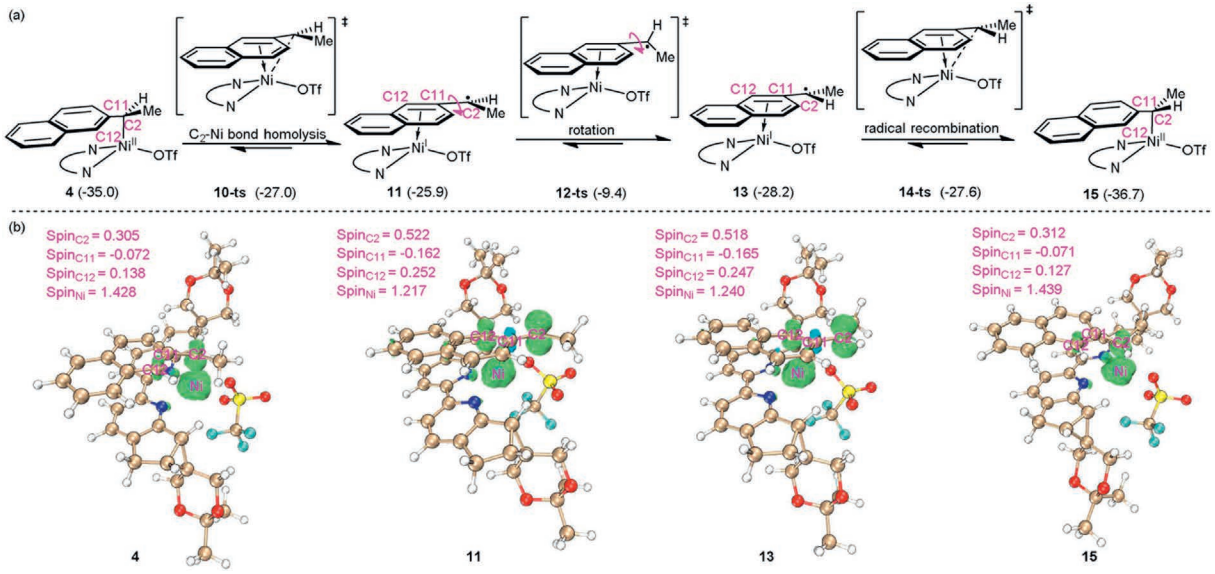


Fig. 2. (a) Pathway of C2–Ni(II) bond homolysis-recombination for the formation of optically pure enantiomeric carbon-metal species (all energies are in kcal/mol). (b) Spin population analysis of intermediates and transition states calculated using Multiwfn 3.8 (dev) software.

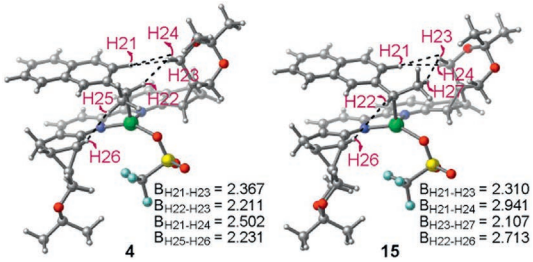


Fig. 3. Optimized geometries of **4** and **15**, and the H···H distance between the substrate and ligand in **4** and **15** (all distances are given in angstroms).

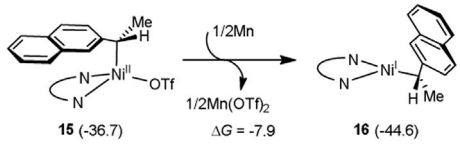


Fig. 4. Reduction of Ni(II) species to Ni(I) species by Mn.

the process is kinetically feasible (Fig. S7 in Supporting information). These results mean C–C• bond rotation can take place, establishing a pre-equilibrium between the **13** and **11** species [66]. The endergonic process makes it difficult for the transient radical to be released, thus enabling rapid recombination and aromatization between the benzyl radical and Ni(I) center. This step generates benzyl Ni(II) complex **15** *via* aryl-ring coordinated recombination transition state **14-ts** forming C–Ni bond, which has an energy barrier of 0.6 kcal/mol. Both geometry and spin population analysis reveal the radical character of benzyl fragment in **11** and **13**, indicating the possible homolysis and radical recombination. Since **15** is 1.7 kcal/mol more stable than **4**, this makes the process of C2–Ni bond homolysis-recombination thermodynamically favorable and benzyl Ni(II) complex **15** is regarded as the major one in the reaction system (Fig. 2). This benzyl radical involved transformation can also be supported by the concept of radical buffering because of the high stability of benzyl radical [67]. By comparing the H···H distances between the substrates and ligands of intermediates **4** and **15** (Fig. 3), we observed that the distance of H12···H24 in **4** is 2.502 Å, whereas in **15**, the distance of H21···H24 is 2.941 Å. Additionally, the distance of H25···H26 in **4** is 2.231 Å, while in **15**, the distance of H22···H26 is 2.713 Å. These results suggest the H–H repulsion between the substrate and chiral ligand in **4** and **15** may be responsible for stability difference.

Ni(II) complex **15** can undergo one-electron reduction by Mn(0) (Fig. 4). The Gibbs free energy change (ΔG) is −7.9 kcal/mol, indicating that one-electron reduction readily occurs [68].

We also investigated the cleavage process of C2–Ni bond in Ni(I) species **16**. This process proceeds *via* a 1,3-Ni migration transition state **17-ts** with an activation free energy of 13.7 kcal/mol, leading to the formation of Ni(I) species **18**. Geometry analysis shows that the lengths of C2–Ni, C2–C11 and C12–Ni bonds in **18** are 3.573, 1.370 and 2.062 Å, respectively, indicating an η^1-bonding of Ni center (Fig. S5c in Supporting information). Moreover, spin population analysis of **18** shows spin densities of −0.007, 0.003, 0.000 and 0.963 on the C2, C11, C12 and Ni atoms, respectively, which suggests a negotiable radical characteristics of benzyl fragment. These computational results show a significant double bond characteristic of C2–C11 bond in **18**, thus hampering the rotation of C2–C11 bond. As a result, the corresponding transition state **19-ts** requires an energy barrier of 43.5 kcal/mol, suggesting an unlikely rotation process. Therefore, the stero-isomerization process involving the cleavage of C2–Ni bond in Ni(I) species **16** followed by bond rotation would not occur (Fig. 5).

The next step is the carboxylation of **16** with CO_2 for the formation of C–C bond, as shown in the Fig. 6a. In this process, two pathways, including stereoretentive inner-sphere and stereoinvertive outer-sphere pathway were considered [69]. In inner-sphere pathway, approaching of CO_2 generates an η^2-coordinated intermediate **22** with a Ni···CO_2 distance of 1.971 Å and the Wiberg bond order of 0.486, indicating a chelation-assisted CO_2 insertion process. ETS-NOCV analysis reveals a significant back-donation interaction between the $d_{x2\text{-}y2}$ orbital of Ni atom and the unoccupied π^* orbital of CO_2 ($E = -77.9$ kcal/mol), effectively stabilizing the Ni–CO_2 complex and contributing to the activation of CO_2 as well (Fig. 6b). As a result, the C5–O bond in **22** is significantly weakened, accompanied by a decrease in O–C–O bond angle from 180° in free

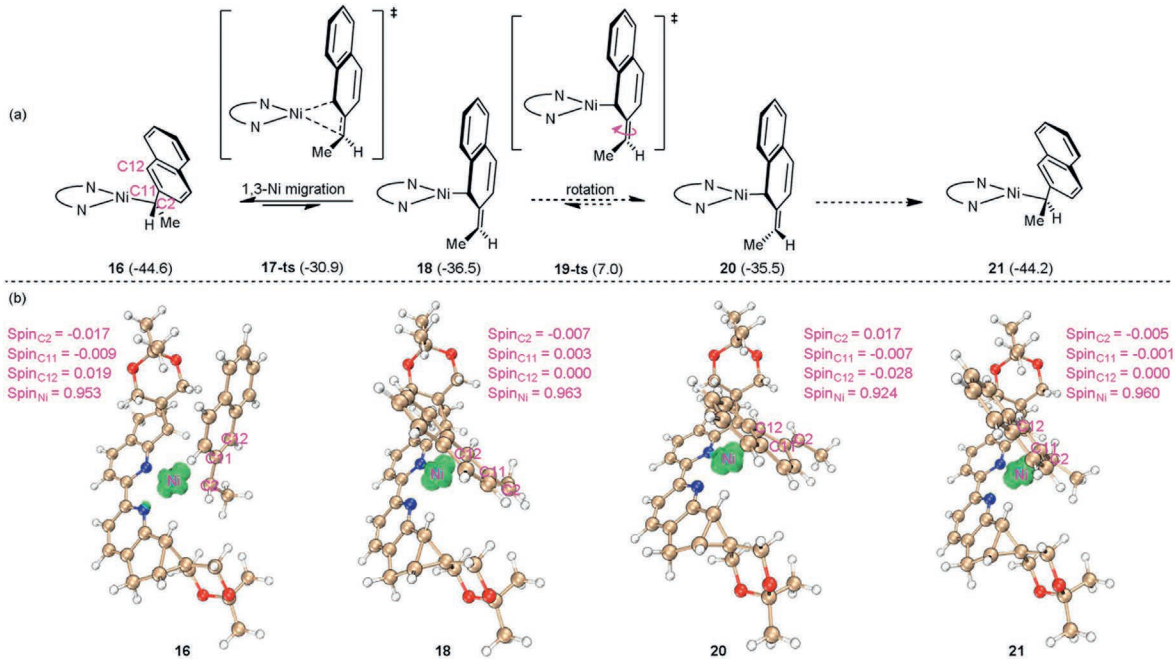


Fig. 5. (a) Process of C2–Ni(I) bond cleavage in Ni(I) species **16** (all energies are in kcal/mol). (b) Spin population analysis of intermediates and transition states calculated using Multiwfn 3.8 (dev) software.

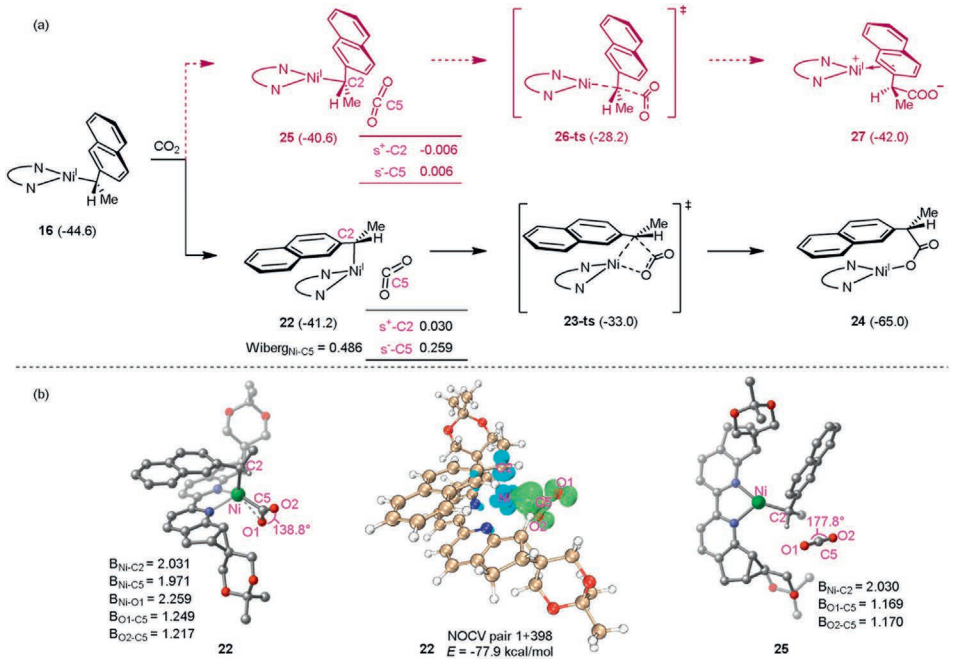


Fig. 6. (a) Comparison of inner-sphere and outer-sphere reaction mechanisms for CO_2 (all energies are in kcal/mol). (b) Optimized geometries of **22** and **25** (all distances are given in angstrom).

CO_2 to 139°. One C=O bond of CO_2 which coordinates with the Ni center becomes somewhat longer to 1.249 Å than that of free CO_2 (1.169 Å). This activation effect also enhances the condensed local softness (s-) [70] of the C5 atom in CO_2, facilitating subsequent C–C bond formation. Thereafter, carboxylation occurs *via* a four-membered ring transition state **23-ts**, generating Ni(I) carboxylate species **24** with the energy barrier of 8.2 kcal/mol. We also investigated the carboxylation proceeds in an outer-sphere pathway. In this case, a molecular complex **25** might be formed, in which CO_2 has no significant interaction with metal center, suggesting a nucleophilic attack on CO_2 by the backside of the C2 atom in **16**. A slight structural deformation is observed in CO_2 fragment, with the O–C–O bond angle changing to 177° and two C=O bonds of CO_2 (1.169 Å, 1.170 Å) being similar to that of free CO_2 (1.169 Å). It means CO_2 was less activated, resulting in the carboxylation *via* an outer-sphere linear transition state **26-ts** has a higher activation free energy (12.4 kcal/mol) than that *via* inner-sphere transition state **23-ts**. Therefore, the outer-sphere pathway can be excluded.

Based on the results above, a comprehensive pathway for the Ni-catalyzed enantioconvergent carboxylation with CO_2 was proposed, with the corresponding energy profiles shown in Fig. 7.

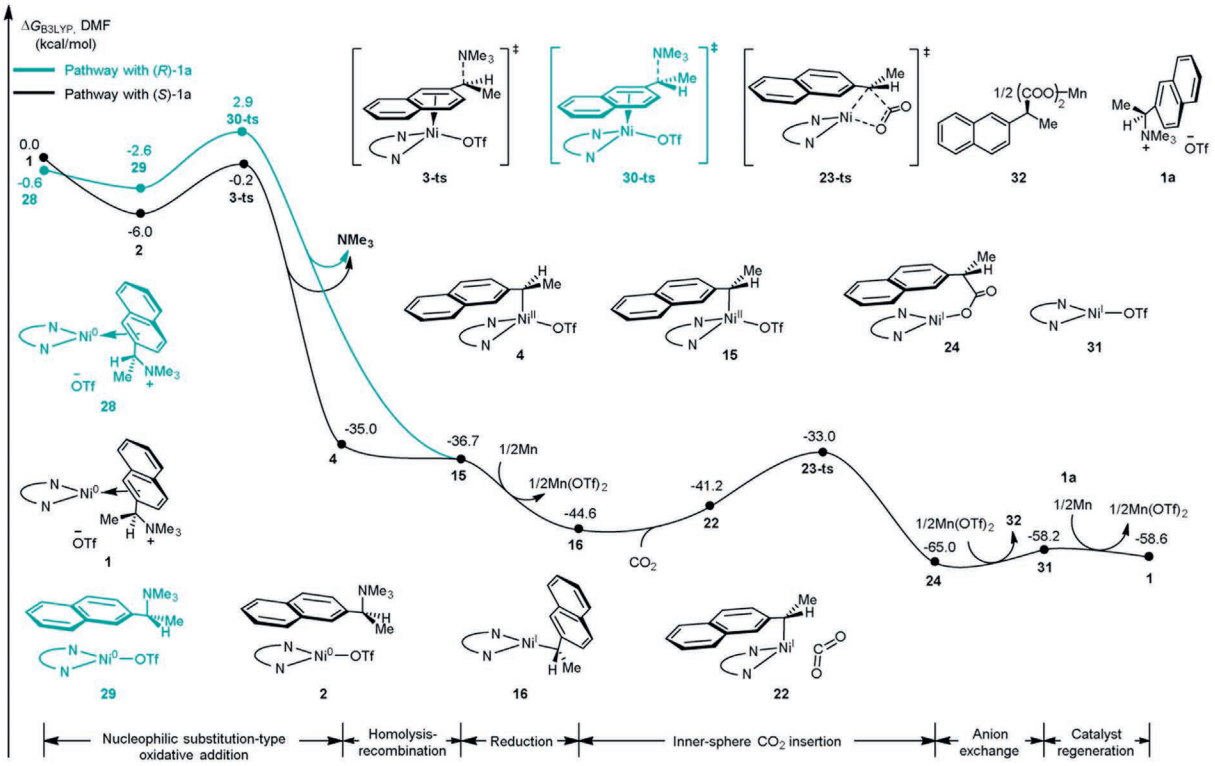


Fig. 7. Energy profiles for Ni-catalyzed enantioconvergent carboxylation of alkyl ammonium salt **1a** with CO_2 (all energies are in kcal/mol).

The Ni(0)-L catalyst ligated with racemic **1a**, generates **1**/**28**. The following nucleophilic substitution-type oxidative addition takes place *via* transition state **3-ts**/**30-ts**. After releasing NMe_3, benzyl Ni(II) complex **4**/**15** was thermodynamically favorably formed. Since **15** is 1.7 kcal/mol more stable than **4**, this makes the process of C(benzyl)–Ni bond homolysis-recombination thermodynamically favorable, enabling the transformation of **4** into **15** as the major one in the reaction system. Once the benzyl Ni(II) species **15** is generated, it can be easily reduced to low-valent Ni(I) species **16** in the presence of excess Mn powder. Subsequent CO_2 insertion into the Ni(I)–C(benzyl) bond of **16** affords the (*S*)-isomeric product, which is consistent with experimental observation. This step *via* inner-sphere transition state **23-ts** requires an activation free energy of 8.2 kcal/mol. After carboxylation, reduction, dissociation of the carboxylate (**1**), and the coordination of the substrate **1a** occur to regenerate the Ni(0) intermediate **1**.

In summary, a carbon–metal bond homolysis/recombination model for Ni-catalyzed enantioconvergent carboxylation of benzyl ammonium salt with CO_2 was proposed and validated. The key step of C(benzyl)–N bond activation by Ni(0) complex is stereoinvertive nucleophilic substitution-type oxidative addition, resulting in the formation of benzyl Ni(II) complex. Then the C–Ni(II) bond homolysis, rotation and recombination might occur giving a more thermodynamically stable stereoisomeric benzyl Ni(II) complex. Subsequent reduction and CO_2 insertion through stereoretentive inner-sphere pathway give the chiral carboxylated product. This model achieves catalytic carboxylation of benzyl (pseudo)halides with CO_2 in high enantioselectivity. The comprehensive mechanistic investigation establishes fundamental principles governing the enantioconvergent catalytic carboxylation of benzyl (pseudo)halides with CO_2, highlighting the potential utility of carbon–metal bond homolysis-recombination protocols in asymmetric reductive cross-coupling reactions. Future experimental and computational studies will further expand the scope and explore the generality of this mechanism.

Declaration of competing interest

The authors declare that they have no known competing financial interests or personal relationships that could have appeared to influence the work reported in this paper.

CRediT authorship contribution statement

Qi Zhou: Writing – original draft, Methodology, Investigation, Formal analysis, Data curation, Conceptualization. **Cefei Zhang:** Writing – original draft, Validation, Investigation, Formal analysis. **Hui-Lin Luo:** Writing – original draft, Investigation, Formal analysis. **Chuan-Xi Nie:** Writing – original draft, Investigation, Formal analysis. **Changwei Hu:** Writing – review & editing, Supervision, Project administration, Formal analysis. **Jian-Heng Ye:** Writing – review & editing, Supervision, Formal analysis. **Zhishan Su:** Writing – review & editing, Supervision, Project administration, Funding acquisition, Formal analysis. **Li-Li Liao:** Writing – review & editing, Supervision, Project administration, Funding acquisition, Formal analysis. **Da-Gang Yu:** Writing – review & editing, Supervision, Project administration.

Acknowledgments

This work was supported by the National Key R&D Program of China (No. 2024YFA1509703), National Natural Science Foundation of China (Nos. 22473081 and 22201027), Fundamental Research Funds from Sichuan University (No. 2020SCUNL102), Sichuan Science and Technology Program (No. 2025ZNSFSC0911), Sichuan University Interdisciplinary Innovation Fund, the Open Research Fund of State Key Laboratory of Coordination Chemistry, School of Chemistry and Chemical Engineering, Nanjing University. We thank Y.-Y. Gui from Sichuan Normal University for valuable discussion and help.

Supplementary materials

Supplementary material associated with this article can be found, in the online version, at doi:10.1016/j.cclet.2025.111429.

References

[1] M.P. Plesniak, H.M. Huang, D.J. Procter, Nat. Rev. Chem. 1 (2017) 0077–0092.
[2] C.P. Jasperse, D.P. Curran, T.L. Fevig, Chem. Rev. 91 (1991) 1237–1286.
[3] M. Yan, J.C. Lo, J.T. Edwards, P.S. Baran, J. Am. Chem. Soc. 138 (2016) 12692–12714.
[4] S.P. Pitre, N.A. Weires, L.E. Overman, J. Am. Chem. Soc. 141 (2019) 2800–2813.
[5] K. Liu, M. Schwenzer, A. Studer, ACS Catal. 12 (2022) 11984–11999.
[6] M. Tomanik, I.T. Hsu, S.B. Herzon, Angew. Chem. Int. Ed. 60 (2021) 1116–1150.
[7] L. Li, L.L. Liao, D.G. Yu, et al., Chin. Chem. Lett. 35 (2024) 110104.
[8] S.P. Morcillo, Angew. Chem. Int. Ed. 58 (2019) 14044–14054.
[9] P. Sivaguru, Z. Wang, G. Zanoni, X. Bi, Chem. Soc. Rev. 48 (2019) 2615–2656.
[10] S.W.M. Crossley, C. Obradors, R.M. Martinez, R.A. Shenvi, Chem. Rev. 116 (2016) 8912–9000.
[11] S.M. Bhutto, R.X. Hooper, P.L. Holland, et al., Chem. Sci. 15 (2024) 3485–3494.
[12] Y.F. Sun, B.C. Wang, Z. Lu, et al., ACS Catal. 14 (2024) 8405–8413.
[13] J.B. Diccianni, T. Diao, Trends. Chem. 1 (2019) 830–844.
[14] C.S. Zhang, B.B. Zhang, Z.X. Wang, et al., Chem. Sci. 13 (2022) 3728–3739.
[15] R. Poli, Comptes Rendus. Chimie 24 (2021) 147–175.
[16] G.Y. Han, P.F. Su, X.Z. Shu, et al., Nat. Catal. 7 (2024) 12–20.
[17] D. Wu, W.Y. Kong, G.Y. Yin, et al., Nat. Catal. 6 (2023) 1030–1041.
[18] N. Kielland, C.J. Whiteoak, A.W. Kleij, Adv. Synth. Catal. 355 (2013) 2115–2138.
[19] D. Ghosh, S. Dabas, S. Subramanian, et al., Catal. Sci. Technol. 15 (2025) 618–646.
[20] C.K. Ran, X.W. Chen, D.G. Yu, et al., Sci. China Chem. 63 (2020) 1336–1351.
[21] Y. Shi, B.W. Pan, F. Zhou, et al., Org. Biomol. Chem. 18 (2020) 8597–8619.
[22] X. Guo, Y. Wang, J.B. Xia, et al., Chin. J. Org. Chem. 40 (2020) 2208–2220.
[23] D. García-Lopez, L. Pavlovic, K.H. Hopmann, Organometallics 39 (2020) 1339–1347.
[24] L. Pavlovic, M. Pettersen, K.H. Hopmann, et al., Eur. J. Org. Chem. (2021) 663–670 2021.
[25] M. Pettersen, K.H. Hopmann, A. Bayer, et al., Adv. Synth. Catal. 366 (2024) 2976–2986.
[26] X.W. Chen, Y. Lan, D.G. Yu, et al., J. Am. Chem. Soc. 141 (2019) 18825–18835.
[27] M. Takimoto, Y. Nakamura, K. Kimura, M. Mori, J. Am. Chem. Soc. 126 (2004) 5956–5957.
[28] S. Kawashima, K. Aikawa, K. Mikami, Eur. J. Org. Chem. (2016) 3166–3170 2016.
[29] X.W. Chen, J.P. Yue, D.G. Yu, et al., Angew. Chem. Int. Ed. 60 (2021) 14068–14075.
[30] X.W. Chen, J.H. Ye, D.G. Yu, et al., Angew. Chem. Int. Ed. 63 (2024) e202403401.
[31] Q. Hu, D.G. Yu, C. Guo, et al., J. Am. Chem. Soc. 146 (2024) 14864–14874.
[32] C. Li, X.W. Chen, Y. Lan, D.G. Yu, et al., Angew. Chem. Int. Ed. 64 (2025) e202413305.
[33] Y.Y. Gui, N.F. Hu, D.G. Yu, et al., J. Am. Chem. Soc. 139 (2017) 17011–17014.
[34] Y.Y. Gui, J.H. Ye, D.G. Yu, et al., J. Am. Chem. Soc. 146 (2024) 2919–2927.
[35] L. Zhou, L. Li, Y. Tang, et al., J. Am. Chem. Soc. 146 (2024) 18823–18830.
[36] S.D. Zhang, L.P. Li, Y. Tang, et al., J. Am. Chem. Soc. 146 (2024) 2888–2894.
[37] B.H. Ye, L. Su, J.W. Liu, et al., Angew. Chem. Int. Ed. 64 (2025) e202413949.
[38] Y.Y. Gui, X.W. Chen, J.P. Yue, D.G. Yu, Chem. Synth. 4 (2024) 66.
[39] Y.Y. Gui, X.W. Chen, D.G. Yu, Chin. J. Org. Chem. 44 (2024) 1038–1040.
[40] L.H. Wang, T. Li, P.F. Li, et al., Angew. Chem. Int. Ed. 61 (2022) e202213943.
[41] T. Moragas, M. Gaydou, R. Martin, Angew. Chem. Int. Ed. 55 (2016) 5053–5057.
[42] M.J. Frisch, G.W. Trucks, H.B. Schlegel, et al., Gaussian 09, Gaussian, Inc., Wallingford, CT, USA, 2013 Revision D.01.
[43] P.J. Stephens, F.J. Devlin, C.F. Chabalowski, M.J. Frisch, J. Phys. Chem. 98 (1994) 11623–11627.
[44] S. Grimme, S. Ehrlich, L. Goerigk, J. Comput. Chem. 32 (2011) 1456–1465.
[45] P.J. Hay, W.R. Wadt, J. Chem. Phys. 82 (1985) 270–283.
[46] W.R. Wadt, P.J. Hay, J. Chem. Phys. 82 (1985) 284–298.
[47] P.J. Hay, W.R. Wadt, J. Chem. Phys. 82 (1985) 299–310.
[48] M.M. Francl, W.J. Pietro, M.S. Gordon, J. Chem. Phys. 77 (1982) 3654–3665.
[49] A.V. Marenich, C.J. Cramer, D.G. Truhlar, J. Phys. Chem. B 113 (2009) 6378–6396.
[50] C. Gonzalez, H.B. Schlegel, J. Chem. Phys. 90 (1989) 2154–2161.
[51] M. Dolg, U. Wedig, H. Stoll, H. Preuss, J. Chem. Phys. 86 (1987) 866–872.
[52] R. Krishnan, J.S. Binkley, R. Seeger, J.A. Pople, J. Chem. Phys. 72 (1980) 650–654.
[53] C.Y. Legault, 2020 (http://www.cylview.org).
[54] A.E. Reed, F. Weinhold, J. Chem. Phys. 78 (1983) 4066–4073.
[55] J.P. Foster, F. Weinhold, J. Am. Chem. Soc. 102 (1980) 7211–7218.
[56] T. Ziegler, A. Rauk, Theor. Chim. Acta 46 (1977) 1–10.
[57] M. Mitoraj, A. Michalak, J. Mol. Model. 13 (2007) 347–355.
[58] A. Michalak, M. Mitoraj, T. Ziegler, J. Phys. Chem. A 112 (2008) 1933–1939.
[59] M.P. Mitoraj, A. Michalak, T. Ziegler, J. Chem. Theory. Comput. 5 (2009) 962–975.
[60] T. Lu, F. Chen, J. Comput. Chem. 33 (2012) 580–592.
[61] W. Humphrey, A. Dalke, K. Schulten, J. Mol. Graph. 14 (1996) 33–38.
[62] T. Moragas, A. Correa, R. Martin, Chem. Eur. J. 20 (2014) 8242–8258.
[63] R.G. Tian, L.Y. Wang, L.Z. Zheng, S.K. Tian, ACS Catal. 14 (2024) 5039–5046.
[64] Q. Lin, Y. Fu, P. Liu, T.N. Diao, J. Am. Chem. Soc. 143 (2021) 14196–14206.
[65] J. Liu, Y. Yang, K. Ouyang, W.X. Zhang, Green Synth. Catal. 2 (2021) 87–122.
[66] S. Lee, H. Ki, H. Ihee, et al., Nat. Commun. 16 (2025) 1969.
[67] M.H. Xu, Y.B. Li, H. Wang, F. Glorius, X.T. Qi, Angew. Chem. Int. Ed. (2025) e202500522.
[68] H. Ryu, B. Pudasaini, M.H. Baik, et al., Chem. Sci. 13 (2022) 10707–10714.
[69] S.Q. Zhang, X. Hong, Acc. Chem. Res. 54 (2021) 2158–2171.
[70] R.K. Roy, S. Krishnamurti, P. Geerlings, S. Pal, J. Phys. Chem. A 102 (1998) 3746–3755.